ЖУРНАЛ СТРУКТУРНОЙ ХИМИИ

2015. Том 56, № 1 *Январь – февраль* *С. 49 – 58*

UDC 543.422:547.12

CRYSTAL STRUCTURE, SPECTROSCOPY, AND THEORETICAL CALCULATIONS OF TWO BIS(BENZIMIDAZOLYL)BUTANE DERIVATIVES

G.-Y. Li[1], J.-S. Hu[1], Y.-F. Liu[2], G.-H. Cui[1]

[1]*College of Chemical Engineering, Hebei United University, Tangshan, P. R. China*
[2]*College of Physics and Electronical Engeering, Henan Normal University, Xinxiang, P. R. China*
E-mail: tscghua@126.com

Received May, 18, 2013

Two ligands for coordination compounds incorporating benzimidazole moieties, namely 1,1′-butane-1,4-diylbis(5,6-dimethyl-1H-benzimidazole) and 1,1′-butane-1,4-diylbis(1H-benzimidazole), are synthesized and then characterized both experimentally and theoretically. Their structures are studied by single crystal X-ray diffraction, UV-Vis spectroscopy, and FT-IR spectroscopy. The optimized geometries, vibrational frequencies, vertical excitation energies of the two ligands are calculated using the (TD)DFT/B3LYP/TZVP method. The calculated results reproduce the experimental data. Additional bonding information about the coordinated N atoms in the two ligands is obtained by FMO and NBO analysis to investigate the substitute-group effect on the coordination ability. The results confirm that the ligand with electron-donating methyl groups on the benzimidazole moieties has a stronger coordination ability.

K e y w o r d s: coordination polymer, benzimidazole, crystal structure, DFT, NBO.

INTRODUCTION

A coordination polymer (CP), also called the metal organic framework (MOF), was first systematically studied by Australian chemist R. Robson in around 1990 [1, 2]. Nowadays, the research of CPs has been rapidly developed and became an important field of coordination supermolecular chemistry. CP materials are potentially applied to gas adsorption and separation [3], molecular recognization [4, 5], heterogeneous catalysis [6], electrical conduction [7], biomedical imaging [8, 9], and drug delivery [10]. Unlike traditional organic or inorganic materials, CPs can be rationally designed and synthesized due to their modular nature. They are involved in inorganic-organic hybrid materials which can be fine designed and incorporated of various functionalities at the molecular level [11, 12]. With a combination of crystal engineering and synthetic chemistry, CP structures are 1D, 2D, and 3D infinite [13]. All of them are composed of metal ions (or metal ion clusters) and organic bridging ligands.

The structure of a CP material is mainly determined by the coordination geometry of the bridging ligands and highly directional metal-ligand coordination bonds. The coordination modes of the ligand play an important role in the construction of CPs [14]. Thus, a selection of a suitable organic ligand with certain flexibility is crucial to the construction of CPs. Bis(benzimidazolyl)alkane derivatives were widely used as bridging ligands to construct CP materials [14—16]. In 2012, our group have synthesized two 1D bis(benzimidazole)-based CPs. Different supramolecular structures were obtained by only a subtle change in the substituted group of the benzimidazole moiety [15]. We have also synthesized some other CPs with flexible bis(benzimidazole) ligands. The results showed that the assembly of CPs could be affected by the spacer length of the ligands and the connecting mode [16]. These

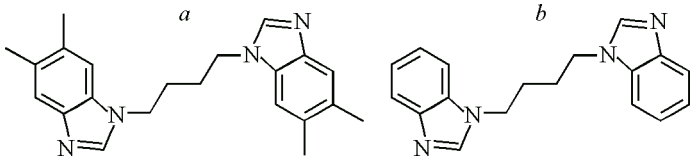

Fig. 1. Structures of (*a*) the ligand **a** and (*b*) the ligand **b**

applications of benzimidazole have led us to investigate the coordination behaviour of different substituted benzimidazole derivatives with transition metal ions.

It is known that substituents bonded to the benzimidazole moiety could influence the electronic characteristics of the ring by either donating electrons or withdrawing electrons. In this way, the coordination behavior of substituted benzimidazole could be modified by substituent effects. In this article, we have synthesized two flexible bis(benzimidazole)-based ligands for the CP synthesis: 1,1′-butane-1,4-diylbis(5,6-dimethyl-1H-benzimidazole) and 1,1′- butane-1,4-diylbis(1H-benzimidazole) (short for *a* and *b*, Fig. 1). Each of them is experimentally characterized by infrared and UV-Vis spectroscopy. The single crystal X-ray diffraction is performed for the ligand **a**, and the crystal structure of the ligand **b** could be obtained from the literature [17]. By comparing their spectra and structures, the substituent effects on the coordination behaviours could be investigated.

In order to understand the substituent effect on the coordination behaviour, the electronic structures of **a** and **b** must be theoretically evaluated. Density functional theory (DFT) and time-dependent density functional theory (TDDFT) could be used to demonstrate the electronic structure and photophysical properties of **a** and **b**. We have focused our attention on the comparison of DFT and TDDFT calculations with experimental observations. In addition, the natural bonding orbitals (NBO) analysis was also carried out in order to explore the bond type and Lewis structure of the two ligands. Thereby the coordination abilities of **a** and **b** could be determined.

EXPERIMENTAL AND COMPUTATIONAL METHODS

Synthesis. All the reagents and solvents for synthesis were purchased from commercial sources and used without further purification. The ligands **a** and **b** were prepared according to the literature [17].

Apparatus. The infrared (IR) spectrum was recorded from KBr pellets in the range 4000—400 cm^{-1} on a Nicolet FT-IR 170SX spectrometer. UV-Vis spectra of **a** and **b** were obtained with the Hitachi UV-3600 spectrophotometer in a methanol solution (2.0×10^{-5} mol/dm^3) at 298 K.

X-ray crystallographic studies of the complex. A suitable single crystal of the title complex ligand **a** was mounted on glass fibers for the X-ray measurement. Reflection data were collected at room temperature (25°C) on a Bruker Smart 1000 CCD diffractometer with graphite-monochromated MoK_α radiation (λ = 0.71073 Å) and an ω-2θ scan mode. Unit cell constants and the orientation matrix were improved by the least squares refinement of reflections thresholded from the entire dataset. Integration was performed with SAINT, using this improved unit cell as a starting point. Precise unit cell constants were calculated in SAINT from the final merged dataset. All the measured independent reflections were used in the structure analyses, and semi-empirical absorption corrections were applied using the SADABS program [18]. The crystal structure was solved by the direct method and subsequently completed by the difference Fourier recycling. All the non-hydrogen atoms were refined anisotropically using the full-matrix, least squares technique. All the hydrogen atoms were positioned geometrically and refined using a riding model for the title complex. All the calculations were performed using the SHELXTL and SHELXL-97 programs [19]. The crystallographic data and experimental details of the data collection and the structure refinement are given in Table 1.

Computational Details. All calculations on electronic structures of ligand **a** and **b** were carried out using the Gaussian 09 [20] program package. Geometry optimizations and the vibration analysis were performed using DFT and the absorption spectrum was calculated using the TDDFT method.

Table 1

Crystal data and structure refinement for the ligand **a**

Empirical formula	$C_{22}H_{26}N_4$
Formula weight	346.47
Wavelength, Å	0.71073
Crystal system	*P*21/*c*
Space group	Monoclinic
a, *b*, *c*, Å	6.160(10), 7.768(13), 18.90(3)
α, β, γ, deg.	90, 99.38(4), 90
V, Å^3	892(3)
Z	2
D_c, g/cm^3	1.228
Crystal size, mm	0.19×0.17×0.15
θ range, deg.	1.09 to 25.02
F(000)	372
Limiting indices	$-7 \le h \le 7$, $-9 \le k \le 6$, $-22 \le l \le 20$
Reflections collected	4462
Independent reflections	1631
R_{int}	0.1070
Completeness to θ = 25.02, %	99.6
Absorption coefficient, mm^{-1}	0.078
T, K	295(2)
GOOF on F^2	0.893
Final *R* indices [$I > 2\sigma(I)$]	$R_1 = 0.0933$, $wR_2 = 0.2242$
R indices (all data)	$R_1 = 0.1793$, $wR_2 = 0.2822$
$\Delta\rho_{max}$ / $\Delta\rho_{min}$, e/Å^{-3}	0.273 / –0.356

Becke′s three-parameter hybrid exchange functional with the Lee—Yang—Parr gradient-corrected correlation (B3LYP functional) [21—25] was chosen as the functional. The triple-ξ valence quality with one set of polarization functions (TZVP) [26] was chosen as basis sets throughout, which is an appropriate basis set for such organic compounds [27]. No constrains for symmetry, bonds, angles, or dihedral angles were applied in the geometry optimization calculations. All of the local minima were confirmed by the absence of an imaginary mode in vibrational analysis calculations. Furthermore, the NBO analysis [28] was performed using the NBO 3.1 program implemented in the Gaussian 09. A useful aspect of the NBO method is that it gives information about interaction in both filled and virtual orbital spaces. The NBO analysis is already proved to be an effective tool for the chemical interpretation of the electron density distribution of the lone electron pair.

RESULTS AND DISCUSSION

Crystal structure and geometry optimization. The single crystal X-ray structural analysis of the ligand **a** reveals that it crystallizes in the monoclinic space group *P*21/*c* (Fig. 2). The dihedral angle between two benzimidazole moieties is close to 0°, showing that they are almost parallel. The bond lengths and angles in the ligand **a** are all within a normal range (Table 2). The N1—C1 and N2—C1 bond lengths are not equal in the 5,6-dimethylbenzimidazole moiety. The N1—C1 (1.299(9) Å) length is shorter than the N2—C1 length (1.396(8) Å), which indicates that the N1—C1 bond is close to the double bond and the N2—C1 bond is close to the single bond. These distances are comparable with those found for many benzimidazole derivatives [29, 30]. As reported, N1—C1 and N2—C1 bond lengths are 1.3079 (14) Å and 1.3564 (13) Å respectively [17] in the ligand **b**. The data indicate that

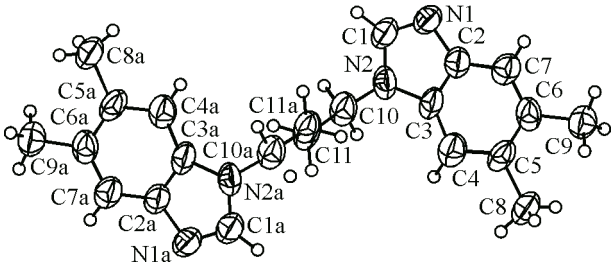

Fig. 2. The atom numbering scheme from single crystal X-ray diffraction and displacement ellipsoids drawn at the 50 % probability level.
Symmetry code: (*i*) 1–*x*, –*y*+2, –*z*

the N1—C1 bond order is higher than that of N2—C1 in both **a** and **b**. The methyl groups have a slight effect on their molecular structures.

The optimized structures of the ligands **a** and **b** shown in Fig. 3 are obtained by the B3LYP functional with TZVP basis sets. The optimization is started from their crystal structures in order to avoid local minima. As shown in Table 2, all the calculated structural parameters of the ligand **a** are nearly equal to the single crystal data. For instance, the calculated N1—C1 and N2—C1 distances in the ligand **a** are 1.30 Å and 1.37 Å respectively, which is in good agreement with the experimental values of 1.299(9) Å and 1.365(10) Å. Especially, the calculation predicts an N2—C10—C11—C11 dihedral angle α of 11°, whereas the experimental value of 63° was found. We attribute the difference to the fact that the experimental studies are performed in the solid crystal phase and the optimizations are performed in the gas phase. The intermolecular interactions in the crystal have connected the molecules together, which results in the differences of structural parameters in the calculated and experimental values. The calculated geometry of the ligand **b** also reproduces its crystal structure. The bond length differences of the ligand **b** between the experimental and theoretical data are not more than 0.02 Å and the differences in the bond and dihedral angles are not more than 2°. Herein, the geometries of the ligands **a** and **b** are very close. Substituents could make little influence on the structures of **a** and **b**.

The molecular electrostatic potential (MEP) is a useful descriptor in understanding the sites for coordination. In order to visualize the coordination sites, MEP of the ligands **a** and **b** was calculated.

T a b l e 2

Comparison of bond lengths (Å) *and angles* (deg.) *for the ligands* **a** *and* **b** *from single crystal* X-*ray diffraction data and* DFT *calculations*

Parameter	Ligand **a**		Ligand **b**	
	Crystal data	DFT data	Crystal data[a]	DFT data
N(1)—C(1)	1.299(9)	1.30	1.3079(14)	1.30
C(3)—N(2)	1.379(8)	1.38	1.3772(13)	1.39
N(1)—C(2)	1.396(8)	1.39	1.3853(13)	1.39
N(2)—C(1)	1.365(10)	1.37	1.3564(13)	1.37
N(2)—C(10)	1.449(9)	1.45	1.4597(13)	1.45
N(1)—C(1)—N(2)	112.4(6)	114.2	114.40(9)	114.2
N(2)—C(3)—C(2)	103.4(7)	105.2	105.04(8)	105.0
C(1)—N(1)—C(2)	105.4(7)	104.6	103.98(8)	104.7
C(3)—N(2)—C(1)	108.6(7)	106.7	106.30(8)	105.9
C(7)—C(2)—N(1)	130.3(9)	130.1	130.29(9)	129.9
N(1)—C(2)—C(3)	110.1(6)	110.3	110.27(9)	110.1
C(1)—N(2)—C(10)	125.2(6)	126.8	127.13(9)	126.7
N(2)—C(3)—C(4)	135.1(9)	133.1	132.15(9)	132.7
N(2)—C(10)—C(11)	115.5(6)	114.1	111.88(9)	113.3

[a] From Ref [17].

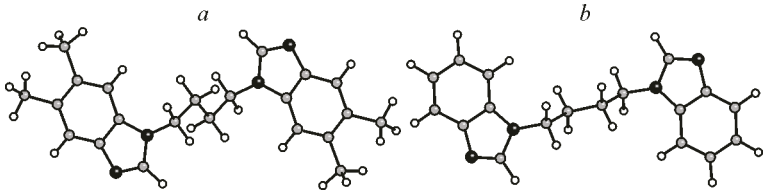

Fig. 3. Optimized geometries of (*a*) the ligand **a** and (*b*) the ligand **b** obtained from DFT calculations

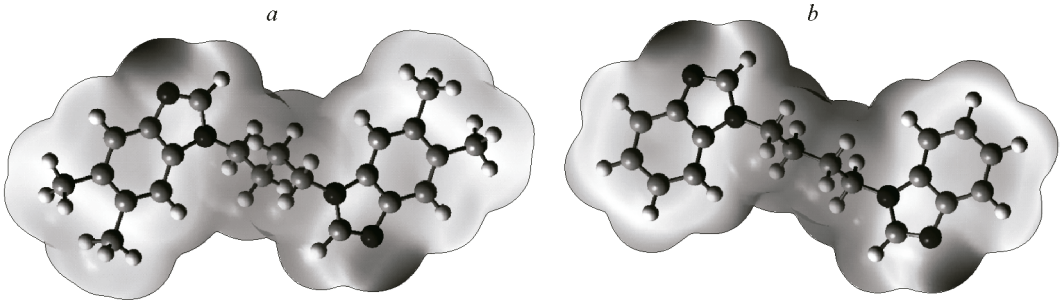

Fig. 4. MEPs of (*a*) the ligand **a** and (*b*) the ligand **b**

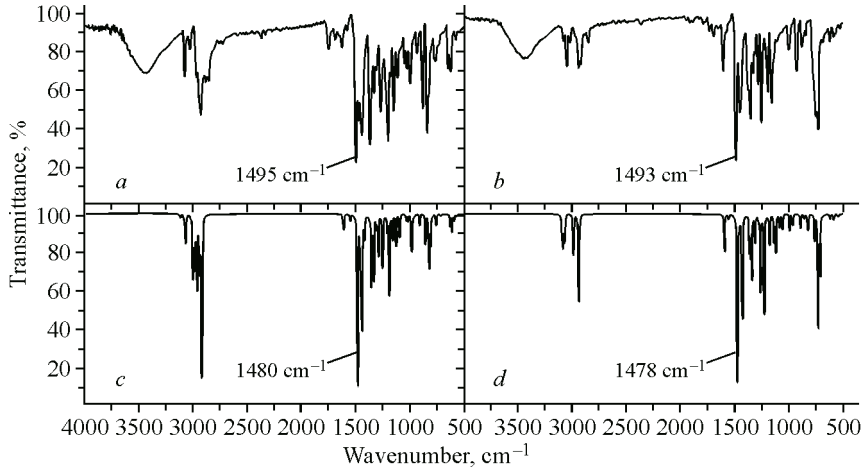

Fig. 5. Comparison of the experimental and calculated IR spectra of **a** and **b**. (*a*)/(*b*) Experimental IR spectra of **a**/**b**. (*c*)/(*d*) Scaled vibration frequencies of **a**/**b** using the DFT method

As shown in Fig. 4, the red color indicates the negative regions and the blue color indicates the positive regions. It is noted that the N1 atom is the most negatively charged atom in either **a** or **b**. This can explain why N1 is the coordination atom in the two organic bridging ligands.

FT-IR spectrum and vibration analysis. IR spectroscopy is widely used to study the structural aspects of organic molecules. Fig. 5, *c*, *d* presents the FT-IR spectra in the range 4000—400 cm^{-1} of **a** and **b**. We also calculated the vibrational frequencies of two ligands at their optimized structures in order to assign the IR peaks (Fig. 5, *a*, *b*). The results of the frequency analysis revealed no imaginary frequencies, indicating that stationary geometries were found. The partial observed and calculated data are summarized in Table 3. As shown in Fig. 5, the calculated and experimental spectra show a minor difference. There are two factors that may be responsible for the discrepancies. Firstly, the calculated DFT harmonic frequencies tend to overestimate the vibrational frequencies because of improper dissociation behavior [31]. Thus, the calculated data of vibration analysis are often lager than those ob-

T a b l e 3

Comparison of the observed and calculated vibrational frequencies (cm^{-1}) *of* **a** *and* **b**

Ligand	Exp.		Cal.			Vib. feature
	Freq.	Int.(IR)[a]	Nonscaled	Scaled[b]	Int.(IR)	
a	3076	m	3185	3075	15	ν(=C—H)
	2925	s	3023	2919	147	ν(—CH_3)
	1495	vs	1533	1480	179	ν(C1—N1, C2—N2)
	1444	m	1489	1438	106	δ(—CH_2—)
	1365	m	1401	1352	70	δ(—CH_2—)
	1203	s	1231	1189	85	δ(—CH_2—)
	841	m	869	839	31	δ(=C—H)
b	3050	m	3151	3042	32	ν(=C—H)
	2930	m	3030	2926	92	ν(—CH_2—)
	1493	vs	1531	1478	174	ν(C1—N1, C2—N2)
	1443	m	1482	1431	107	δ(—CH_2—)
	1357	m	1391	1343	64	δ(—CH_2—)
	1235	s	1273	1229	100	δ(—CH_2—)
	734	m	758	732	107	δ(=C—H)

[a] m — middle, s — strong, vs — very strong.
[b] Scaling factor: 0.9654 [31].

tained from the IR spectrum. The calculated data are modified using 0.9654 [31] as the frequency scaling factor for the B3LYP/TZVP method. Secondly, the experimental spectra are performed in the solid state, while the calculated spectra correspond to isolated molecules in the gas phase.

In Fig. 5, it can be seen that the calculated frequency data of **a** and **b** well reproduce their IR spectra. The experimental vibrational bands at approximately 3400 cm^{-1} in Fig. 5, *c*, *d* are assigned to *ν*(OH) of water, which do not appear in the computed spectra in Fig. 5, *a*, *b*. The IR spectrum of the ligand **a** shows a band at 1495 cm^{-1}, which is one of the characteristic vibrations of imidazole [32]. For the ligand **b** there is a band at 1493 cm^{-1}, nearly equal to that of **a**. The corresponding bands have been computed as 1533 cm^{-1} in the ligand **a** and 1531 cm^{-1} in the ligand **b**. Both of them are asigned to the N—C—N stretching mode in the imidazole moiety. The results also indicate that the methyl groups have little effect on the N1—C1 bond. Moreover, the experimental bands at more than 3000 cm^{-1} in **a** and **b** coincide with the computed data, which can be assigned to the unsaturated C—H stretching modes. Due to the four methyl groups in **a**, the strong vibration of C—H stretching at 2925 cm^{-1} (cal. 2919 cm^{-1}) is shown.

UV-Vis spectrum and calculated absorption spectrum. We have measured the UV-Vis spectra of the ligand **a** and **b** to study their photophysical characters. Their concentrations are 2.0×10^{-5} mol/l in the methanol solution in the measurements. In order to determine the transition type of these absorption bands, we calculated their vertical excitation energies with the TDDFT approach. The absorption profiles are then calculated using the Gauss models. Frontier molecular orbital (FMO) theory has also been used to provide an explanation for the electron transition in the UV-Vis spectra [33]. In this theory, the highest occupied molecular orbitals (HOMOs) and lowest unoccupied molecular orbital (LUMOs) play vital roles.

In the UV-Vis spectra, the ligands **a** and **b** show similar profiles. As shown in Fig. 6, *c*, the UV-Vis spectrum of **a** shows three low-lying absorption bands at 291 nm, 285 nm, and 266 nm respec-

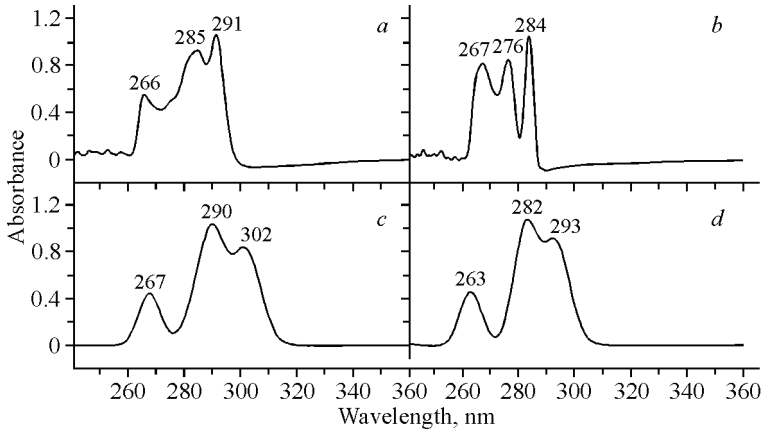

Fig. 6. Comparison of the experimental and calculated UV/Vis spectra. (*a*)/(*b*) Experimental UV/Vis spectra of **a/b** in the methanol solution. (*c*)/(*d*) The calculated absorption bands of **a/b** using the TDDFT method

tively. The calculated absorption bands of **a** are very close to them (Fig. 6, *a*). The calculated transition energies with the highest oscillator strength (*f*, which is a dimensionless quantity to express the strength of the transition) are collected in Table 4 and compared with the experimental data. It reveals that the low-lying band at 291 nm corresponds to the orbital transition from HOMOs to LUMOs and the band at around 285 nm corresponds to HOMO-1s to LUMOs. The UV-Vis spectrum for **b** shows three similar absorption bands in the regions at 284 nm, 276 nm, and 267 nm (Fig. 6, *d*). The calculated results shows three strongest absorption bands of **b** in the UV-region centered at about 293 nm, 282 nm, and 263 nm (Fig. 6, *b*). The transition types of the three bands in **b** are very similar to those in **a**. Compared with the ligand **a**, all the absorption wavelengths of **b** are blue-shifted. This spectral difference can be attributed to the electron-donating effect of methyl groups in **a**.

Fig. 7 lists FMOs involved in the low-lying electronic transitions of **a** and **b**. We can see all of them are doubly degenerate and delocalized over their benzimidazolium moieties. The HOMO-1s of **a** and **b** are mainly composed of the atomic orbital on N1, which are nonbonding orbitals including lone electron pairs. In the case of the ligand **a**, the band at 291 nm is a dominating ππ-type of the transition and the band at 285 nm is generated by the *n*π-type transition. For the ligand **b**, the experimental absorption bands at 284 nm and 276 nm are respectively ππ-type and *n*π-type transitions. Since the LUMO energies and compositions of **a** and **b** are very close, the *n*π-type transition energies could be used to measure the energies of lone electron pairs on their N1 atoms. The HOMO-1s in the ligand **a** have higher energies, which could donate the electron pairs on N1 more easily.

T a b l e 4

Transition energies for the ligands **a** *and* **b** *obtained from both experiment and* TDDFT *calculations*

Ligand	λ_{cal} (nm)	λ_{exp} (nm)	*f*	CI expansion coefficients (>0.2)
a	302	291	0.210	0.380 (HOMO → LUMO)
	290	285	0.253	0.292 (HOMO–1 → LUMO)
	267	266	0.112	0.353 (HOMO → LUMO+1)
b	393	284	0.189	0.367 (HOMO → LUMO)
	282	276	0.230	0.286 (HOMO–1 → LUMO)
	263	267	0.103	0.351 (HOMO → LUMO+1)

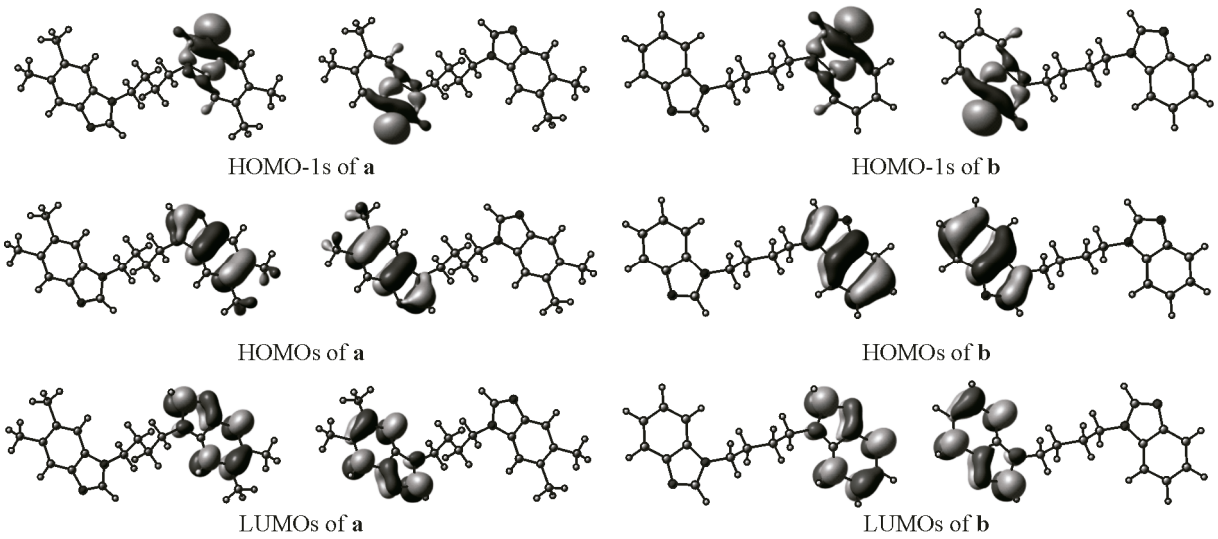

Fig. 7. Frontier molecular orbitals of **a** and **b** related to low-lying electronic transitions obtained from TDDFT calculations (Isovalue = 0.06)

NBO analysis. NBO charge population can help us to understand the bonding properties. As mentioned above, N1 is the coordination atom in the two organic bridging ligands. The natural charges of N1 in **a** and **b** are –0.434 and –0.339 respectively. So the ligand **a** is more likely to coordinate the positively charged central metal ion. Selected results from the natural population analysis for the ligands **a** and **b** are presented in Table 5. Both occupation and hybridization of the orbitals of their N1 atoms are analyzed. The results show that the lone pair on N1 of **a** have mainly 36 % *s* and 64 % *p* characters and its occupation is 1.92. It is suggested that the lone pair of the N1 atom is an $sp^{1.8}$-hybrid orbital. In the ligand **b**, the lone pair on N1 has mainly 37 % *s* and 63 % *p* characters and its occupation is 1.8. So it is an $sp^{1.7}$-hybrid orbital. Even though the lone pairs of **a** and **b** are both approximately occupied by two electrons, the N1 lone pair of **a** is more occupied than that of **b**. That is to say, the N1 atom of **a** can give more electrons to the central metal atom. In addition, as the *p*-proportion of the orbital increases, the hybrid orbital will keep further away from the nucleus in the atom. The *p*-proportion of the lone pair on N1 of **a** is more than that of **b**. It also indicates that the ligand **a** has a better coordination ability.

T a b l e 5

Characteristics of selected orbitals in the ligands **a** *and* **b** *based on the natural population analysis*

Ligand	Bond orbital	Occupation	Composition, %			Contributions of atoms to the orbital, %
			s	*p*	*d*	
a	BD: N1—C1	1.98				N: 57; C: 43
	BD: N1—C1	1.98				N: 57; C: 43
	BD: N1—C2	1.96				N: 57; C: 43
	LP: N1	1.92	36	64	0	
b	BD: N1—C1	1.98				N: 57; C: 43
	BD: N1—C1	1.95				N: 59; C: 41
	BD: N1—C2	1.96				N: 57; C: 43
	LP: N1	1.85	37	63	0	

A b b r e v i a t i o n s: LP — lone pair; BD — bonding orbital.

CONCLUSIONS

Two benzimidazole-based ligands 1,1′-butane-1,4-diylbis(5,6-dimethyl-1H-benzimidazole) and 1,1′-butane-1,4-diylbis(1H-benzimidazole) were synthesized and characterized by the X-ray measurement, FT-IR spectra, UV-Vis spectra, and DFT/TDDFT calculations. The theoretically calculated values of both bond lengths and bond angles of the DFT optimized structures were compared with the X-ray crystallographic data. The results reveal that the N1 atoms in their respective benzimidazole moieties are bound to the neighbour carbon atoms by a single bond and a double bond. FT-IR and UV-Vis spectra of the two ligands were investigated experimentally. In order to understand the electronic transitions of the compounds, the vibration analysis and TDDFT calculations of the electronic absorption spectra were performed. The differences between the observed and calculated values of most of the fundamental bands are very small. HOMO, LUMO orbital localization and NBO analysis confirm that the ligand **a** has a better coordination ability. That is to say, the electron-donating groups on the benzimidazole moieties are helpful to the coordination with the central metal ion. We hope the results of this study will help researchers to design and synthesize new CP materials.

Acknowledgments. The project was supported by the National Natural Science Foundation of China (11247281) and Excellent Youth Fund of Hebei Province Department of Education, China (Y2012010). We thank the Dalian Branch of the Supercomputing Center of the Chinese Academy of Sciences for computing support.

Supplementary materials. CCDC-923261 contains the supplementary crystallographic data for the ligand **a**. This data can be obtained from the Cambridge Crystallographic Data Center, 12 Union Road, Cambridge CB2 1EZ, UK; Fax: +44-1223-336033; E-mail: deposit@ccdc.cam.ac.uk.

REFERENSES

1. *Hoskins B.F., Robson R.* // J. Amer. Chem. Soc. – 1989. – **111**. – P. 5962.
2. *Hoskins B.F., Robson R.* // J. Amer. Chem. Soc. – 1990. – **112**. – P. 1546.
3. *Horcajada P., Serre C., Grosso D., Boissiere C., Perruchas S., Sanchez C., Ferey G.* // Adv. Mater. – 2009. – **21**. – P. 1931.
4. *Cho W., Lee H.J., Oh M.* // J. Amer. Chem. Soc. – 2008. – **130**. – P. 16943.
5. *Tsuruoka T., Furukawa S., Takashima Y., Yoshida K., Isoda S., Kitagawa S.* // Angew. Chem. Int. Ed. – 2009. – **48**. – P. 4739.
6. *Kerbellec N., Catala L., Daiguebonne C., Gloter A., Stephan O., Bunzli J.-C., Guillou O., Mallah T.* // New J. Chem. – 2008. – **32**. – P. 584.
7. *Batten S.R.* Coordination Polymers: Design, Analysis and Application, RSC Publishing, 2008.
8. *Taylor K.M.L., Jin A., Lin W.* // Angew. Chem. Int. Ed. – 2008. – **47**. – P. 7722.
9. *Rieter W.J., Pott K.M., Taylor K.M.L., Lin W.* // J. Amer. Chem. Soc. – 2008. – **130**. – P. 11584.
10. *Taylor K.M.L., Rieter W.J., Lin W.* // J. Amer. Chem. Soc. – 2008. – **130**. – P. 14358.
11. *Chalati T., Horcajada P., Gref R., Couvreur P., Serre C.* // J. Mater. Chem. – 2011. – **21**. – P. 2220.
12. *Hermes S., Witte T., Hikov T., Zacher D., Bahnmculler S., Langstein G., Huber K., Fischer R.A.* // J. Amer. Chem. Soc. – 2007. – **129**. – P. 5324.
13. *Wells A.F.* Three-dimensional nets and polyhedral. – New York: Wiley-Interscience, 1977.
14. *Feng G.-D., Jiang L., Li Z.-X., Chen Q., Wang X.-L., Shao K.-Z., Sun C.-Y., Li L.-J., Yu J.-H., Su Z.-M.* // Inorg. Chem. Comm. – 2012. – **24**. – P. 247.
15. *Xiao S.-L., Du X., Qin L., He C.-H., Cui G.-H.* // J. Inorg. Organomet. Polym. – 2012. – **22**. – P. 1384.
16. *Jiao C.-H., Geng J.-C., He C.-H., Cui G.-H.* // J. Mol. Struct. – 2012. – **1020**. – P. 134.
17. *Akkurt M., Karaca S., Kücükbay H., Büyükgüngör O.* // Acta Crystallogr. – 2007. – **E63**. – P. o1065.
18. *Sheldrick G.M.* SADABS, University of Göttingen, Germany, 1996.
19. *Sheldrick G.M.* SHELXS97 and SHELXL97, University of Göttingen, Germany, 1997.
20. *Frisch M.J., Trucks G.W., Schlegel H.B., Scuseria G.E., Robb M.A., Cheeseman J.R., Scalmani G., Barone V., Mennucci B., Petersson G.A., Nakatsuji H., Caricato M., Li X., Hratchian H.P., Izmaylov A.F., Bloino J., Zheng G., Sonnenberg J.L., Hada M., Ehara M., Toyota K., Fukuda R., Hasegawa J., Ishida M., Nakajima T., Honda Y., Kitao O., Nakai H., Vreven T., Montgomery J.A. Jr., Peralta J.E., Ogliaro F., Bearpark M., Heyd J.J., Brothers E., Kudin K.N., Staroverov V.N., Kobayashi R., Normand J., Raghavachari K., Rendell A.,*

Burant J.C., Iyengar S.S., Tomasi J., Cossi M., Rega N., Millam J.M., Klene M., Knox J.E., Cross J.B., Bakken V., Adamo C., Jaramillo J., Gomperts R., Stratmann R.E., Yazyev O., Austin A.J., Cammi R., Pomelli C., Ochterski J.W., Martin R.L., Morokuma K., Zakrzewski V.G., Voth G.A., Salvador P., Dannenberg J.J., Dapprich S., Daniels A.D., Farkas O., Foresman J.B., Ortiz J.V., Cioslowski J., Fox D.J. Gaussian 09, Revision A.1, Wallingford CT: Gaussian, Inc., 2009.

21. *Becke A.D.* // J. Chem. Phys. – 1993. – **98**. – P. 5648.
22. *Dirac P.A.M.* // Proc. R. Soc. London Ser. A. – 1929. – **123**. – P. 714.
23. *Vosko S.H., Wilk L., Nusair M.* // Canad. J. Phys. – 1980. – **58**. – P. 1200.
24. *Becke A.D.* // Phys. Rev. A. – 1988. – **38**. – P. 3098.
25. *Lee C., Yang W., Parr R.G.* // Phys. Rev. B. – 1988. – **37**. – P. 785.
26. *Treutler O., Ahlrichs R.J.* // Chem. Phys. – 1995. – **102**. – P. 346.
27. *Li G.-Y., Li Y.-H., Zhang H., Cui G.-H.* // Commun. Comput. Chem. – 2013. – **1**. – P. 88.
28. *Glendening E.D., Reed A.E., Carpenter J.E., Weinhold F.* NBO Version 3.1, TCI, University of Wisconsin: Madison, 1998.
29. *Gilbert J.G., Addison A.W., Prabakaran P., Butcher R.J., Bocelli G.* // Inorg. Chem. Commun. – 2004. – **7**. – P. 701.
30. *Li G.-Y., Geng J.-C., He C.-H., Cui G.-H.* // J. Mol. Struct. – 2013. – **1031**. – P. 56.
31. *Scott A.P., Radom L.* // J. Phys. Chem. – 1996. – **100**. – P. 16502.
32. NIST Chemistry WebBook, NIST Standard Reference Database Number 69, Eds. P.J. Linstrom and W.G. Mallard, National Institute of Standards and Technology, Gaithersburg MD, 20899, http: // webbook.nist.gov (retrieved February 12, 2012).
33. *Cahill K.J., Johnson R.P.* // J. Org. Chem. – 2013. – **78**. – P. 1864.